



Investigation of structural, morphological and optical properties of Nickel-doped Zinc oxide thin films fabricated by co-sputtering

Ozkan Bayram^{1,2} · Emre Sener² · Erdal İgman² · Onder Simsek^{2,3}

Received: 16 November 2018 / Accepted: 20 December 2018 / Published online: 2 January 2019
© Springer Science+Business Media, LLC, part of Springer Nature 2019

Abstract

In this study, it was aimed to grow Nickel doped (0.0 at.%, 0.16 at.%, 0.20 at. % and 0.24 at. %) Zinc Oxide (NZO) thin films on quartz substrates using Magnetron Sputtering technique. NZO thin films were obtained at a temperature of 450 °C, a pressure of 480 m Torr and a deposition time of 30 min. Co-sputtering process for both Ni and ZnO target was performed using two separate power sources. The DC power of the Ni target material was 20, 30 and 40 W, respectively while the radio frequency (RF) power of the Zinc oxide (ZnO) target material was set to 150 W. Using XRD analysis, thin films were found to have polycrystalline morphology, and the average crystallite size changed significantly depending on the increased Ni doping level. The optical Transmittance of the thin films was greater than 90% in the visible region (550 nm), and this value tends to decrease slightly by Ni doping. The optical band gap (E_g) firstly decreased and then slightly increased with the Nickel doping ratio and these values were found to be 3.23 eV, 3.11 eV and 3.15 eV, respectively, with increase of Ni doping.

1 Introduction

Transparent conductive oxides (TCOs) have received great interest in recent years as they play an important role in many different application areas such as ultraviolet light-emitting diodes (UV-LEDs) [1], transparent field-effect transistor (FETs), spintronic devices, photovoltaic solar cells (PVSC) [2], piezo- electric sensors [3], transparent electrodes [4] and optoelectronic components [5–7]. ZnO is a transparent semiconductor with wide band gap of 3.37 eV and large exciton binding energy of 60 meV [8–10]. TCO films, such as ZnO, are widely used as electrode layers in thin film solar cells, since they have a high degree of transparency in the visible wavelength range and high conductivity. Indium tin oxide (ITO) is an important TCO material that is widely used today. However, it is likely that the cost

of this material is too high and may not keep it as an alternative product in the future. ITO is likely to fail to respond to existing technology with production at a limited level, and being a product with high toxicity results in the search for alternative products. ZnO is considered as an alternative to ITO because of its environmentally friendly and excellent optical and electrical properties. These properties of ZnO can be further enhanced by ion addition. In a study by Peng et al. [11] they found that pure ZnO thin films improved optical and electrical properties with indium doping at various ratios. With 0.5 at.% indium doping, the highest efficiency was achieved in terms of these properties. In another study, Madhi et al. [12] examined the optical and electrical properties of calcium-doped ZnO thin films and found that the transmittance of ZnO: Ca films was above 80% and the lowest electrical resistivity was about $5 \times 10^{-3} \Omega \text{ cm}$ [13]. Sung et al. [14], studied zirconium-doped ZnO thin films grown on quartz substrates by RF sputtering technique and investigated the effect of Zr-doping on the optical properties of ZnO. It was found that the optical transparency of the thin films was above 90%, but the optical band gap of the Zr doped ZNO (ZZO) thin films increased with Zr addition.

Various techniques such as magnetron sputtering [15], chemical vapor deposition (CVD) [16], pulsed laser deposition (PLD) [17] and sol gel processes [18] have been used to obtain ZnO thin films [16, 19, 20]. Of these techniques, magnetron-sputtering technique is in the foreground,

✉ Ozkan Bayram
obayram@bayburt.edu.tr

¹ Department of Electrical and Electronics Engineering, Engineering Faculty, Bayburt University, TR-69100 Bayburt, Turkey

² Department of Nanoscience and Nanoengineering, Graduate School of Natural and Applied Sciences, Ataturk University, TR-25240 Erzurum, Turkey

³ Central Application and Research Laboratory (MERLAB), Agri Ibrahim Cecen University, TR-04100 Agri, Turkey

because by using this technique, the coating parameters can be easily controlled, the resulting thickness can be adjusted and the film magnification can be applied to large surfaces [21–23]. In this study, it is aimed to obtain Ni-doped Zinc Oxide thin films in various DC power using magnetron sputtering technique. To the best of our knowledge, any study has been conducted in the literature in which Ni-doped ZnO thin films were obtained by this technique. For this purpose, a detailed analysis of Ni doped ZnO and pure ZnO thin films was discussed and compared with other studies. NZO and pure ZnO thin films were analyzed by XRD, SEM, EDX, RAMAN, UV–Vis and PL spectroscopy.

2 Materials and method

ZnO and Ni target materials, which have 99.99% purity, were purchased from Sigma–Aldrich company, Germany. Magnetron sputtering technique was used to obtain thin films. In this technique, both the ZnO target material and the Ni additive material were fed with 150 W RF power and various (20, 30 and 40 W) DC powers, respectively, with the co-sputtering system. Two processes were carried out to clean the substrate surface. Firstly, the substrates, designed in dimensions of $1 \times 1 \times 0.3 \text{ cm}^3$, were subjected to a wet surface cleaning process. Substrates washed with ethanol and propanol, respectively, in the wet cleaning process were then purged with distilled water. Finally, it was aimed to remove atoms and molecules that cause contamination from the surface of the substrate by creating an Argon (Ar) gas plasma through the RF or DC power supply. The process of obtaining thin film is summarized as follows.

Primarily cleaned substrates were placed in the substrate compartments of the Magnetron Sputtering system. The schematic representation of the Magnetron sputtering system is as shown in Fig. 1. To the vacuum chamber of the system, ZnO and Ni target materials were placed in the target material holder compartment. With the help of a vacuum pump, the base pressure of the system was reduced to 10^{-6} m Torr. Vacuum processing was carried out several times so that the vacuum chamber can be cleaned as much as possible from foreign atoms and molecules. At this pressure value, plasma was created by sending Argon gas by the help of sensitive valve. and surface cleaning of quartz substrates with Argon plasma was carried out. This process was done several times, 5 min periods. Then, Argon gas, adjusted to flow rate of 100 sccm by mass flow controllers, was sent to the vacuum chamber. The DC power of the Ni target was set at 20, 30 and 40 W, respectively, and the RF power for the ZnO target was set to 150 W. The pressure of the vacuum chamber was determined to be 480 m Torr, the substrate temperature was $450 \text{ }^\circ\text{C}$, and the coating duration was 30 min. Experiments

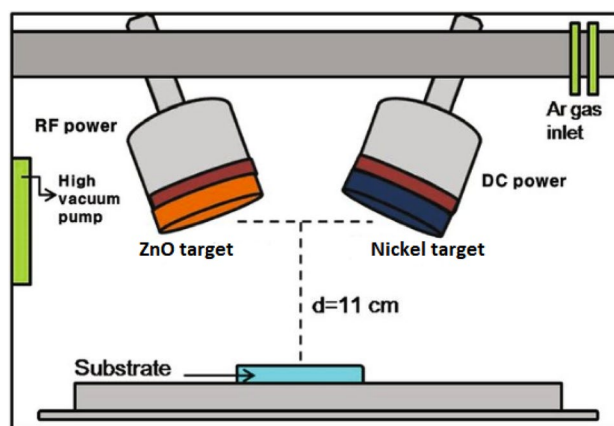


Fig. 1 The schematic representation of the magnetron sputtering system [24]

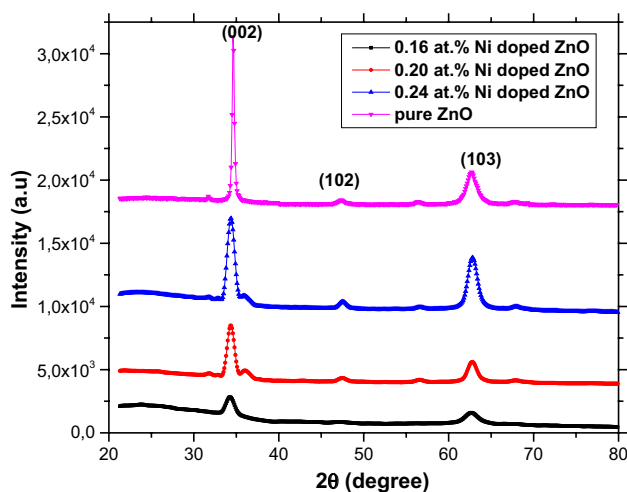


Fig. 2 XRD spectra of NZO thin films

were repeated for each coating and at least five trials were performed for each sample.

3 Results and discussions

3.1 XRD analyses

The crystal structure of pure and Ni doped ZnO was analyzed by X-Ray Diffraction (XRD) method. The XRD patterns of the Nickel-doped and pure ZnO thin films obtained were shown in Fig. 2. Several reflection peaks such as (100), (002), (101), (102) and (103) were found in NZO thin films. For all thin films, XRD results (Ref. JCPDS-Card No. 36-1451) showed that it was hexagonal wurtzite structure with have a preferential c-axis orientation [11, 12, 25, 26]. It is understood from Fig. 2 that the (002) plane is located at

$2\theta = 34.3^\circ$ and the plane (101) is located at approximately $2\theta = 35.3^\circ$. Figure 2 shows that the Ni doping level plays an important role in improving the crystallinity of ZnO thin films. It can be said that the crystallinity of ZnO films with 0.24 at.% Ni is better than that of other films. A similar result was found by Gupta et al. [27], for indium-doped ZnO thin films prepared by the PLD technique. Gupta et al. also noted that much higher indium doping destroyed the crystallinity of ZnO thin films. As a result, the rate of Ni doping has played a vital role in the crystallization of ZnO thin films. As can be seen in Fig. 3, the position of (002) peak shifts slightly to lower angle. This shift might be due to the ionic radius of the Ni^{2+} (0.070 nm) is smaller than that of Zn^{2+} (0.074 nm). In our study, Ni atoms added to pure ZnO lattice structure create crystal stress or defect within the structure.

Crystal defects and stresses are thought to cause significant change in crystal structure. In the XRD spectra, the broadening, narrowing or more intensity of the peaks can be attributed to the crystal structure defects formed by the addition of Ni atoms. Bragg's law is used to determine the interplanar distance (d) and this law is given as follows [28].

$$n\lambda = 2d \sin \theta \quad (1)$$

n is an integer ($n=1$) and θ corresponds to the half-diffraction angle. The distance d of each film for (002) plane is given in Table 1. Table 1 data is in good agreement with standard data (JCPDS No. 36-1451). The average crystallite size (D) for the (002) plane of thin films was calculated using the Debye–Scherrer equation [8].

$$D = \frac{k\lambda}{\beta \cos \alpha} \quad (2)$$

wherein, k, D and λ is, the Scherrer constant of 0.90, the average crystallite size and the wavelength of the X-ray ((0.15406 nm)), respectively. In addition, α is the Bragg

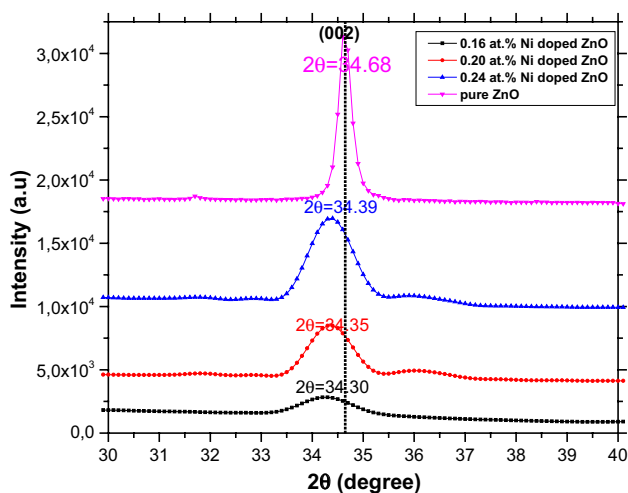


Fig. 3 Position of (002) peak shifts for NZO thin films

Table 1 Some structural parameters of NZO thin films

Ni doping ratios (at.%)	c (\AA)	a (\AA)	$d_{(002)}$ (\AA)	FWHM (degree)	D (nm)
0.00	5.1698	2.9849	2.5849	0.3278	26.53
0.16	5.2246	3.0164	2.6123	1.2334	7.041
0.20	5.2172	3.0091	2.6086	1.0275	8.463
0.24	5.2114	3.0088	2.6057	0.9079	9.578

angle, and β is the full width of the half-maximum (FWHM) of the diffraction peak determined for these angles [29]. D was calculated as 7.041 nm, 8.463 nm, and 9.578 nm with the increase of doping rates for NZO thin films, respectively, while it was 26.53 nm for pure ZnO thin film. In addition, the lattice constants (c) and (a) of the thin films was calculated from the XRD data presented in Table 1 using the following equation [30].

$$\frac{1}{d^2 hkl} = \frac{4}{3} \frac{h^2 + k^2 + hk}{a^2} + \frac{l^2}{c^2} \quad (3)$$

The calculated value of the lattice constant (c) for the pure ZnO thin film is 5.1698 \AA and depending on the increased Ni doping rate, these values are 5.2246 \AA , 5.2172 \AA and 5.2114 \AA for NZO films, respectively. These values calculated for thin films are well agree with standard data (JCPDS No. 36-1451, $c = 5.2066 \text{\AA}$).

Raman spectroscopy was carried out to investigate the microstructure and the vibrational properties of pure and Ni-doped ZnO films. Raman spectroscopy for NZO thin films is shown in Fig. 4. For NZO thin films, E_2 (low) at 97 cm^{-1} , E_2 (high) - E_2 (high) at approximately 374 cm^{-1} , A_1 (TO) mode at 435 cm^{-1} , E_2 (high) mode and A_1 (LO) modes at 565 cm^{-1} were detected. Using the Raman spectrum, the

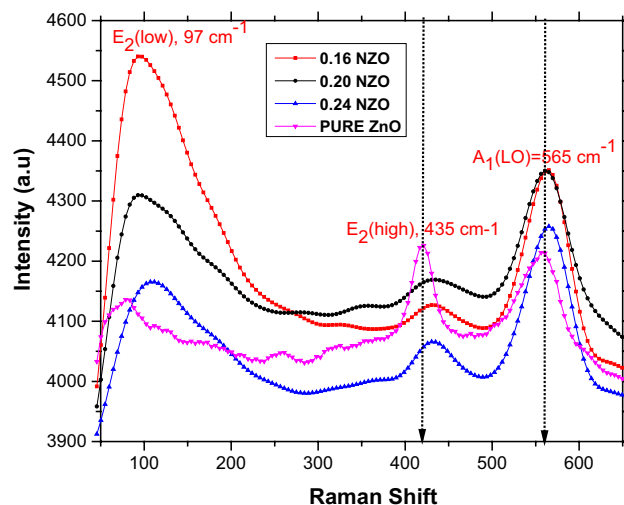


Fig. 4 Raman spectra of NZO thin films

presence of ZnO phonon modes was confirmed. It was understood that these results were in accordance with the studies in the literature [31, 32].

3.2 Optical properties

The optical properties such as absorbance and transmittance spectra of NZO thin films were determined by UV–Vis spectroscopy, and absorbance and transmittance spectra were given in Figs. 5 and 6, respectively. From the absorption spectra, it is seen that the absorption peak of all the NZO samples is centered around at 375 nm and intensity of this peak increases with increase of Ni doping level. As can be seen from Fig. 6, all the thin films are highly transparent (> 90%) in the visible wavelength range, in this respect they are similar to transparent conductive oxides. Also, the transparent of ZnO films with 0.20 and 0.24 at.% Ni is higher than that of ZnO films with 0.16 at.% Ni (at 550 nm). The absorption edges of Ni-doped ZnO thin films shifts to longer wavelengths with increase in Ni content and red shift could be observed similar to previously reported by Chakraborti et al. [33]. and Liu et al. [34]. As it is well known, for the direct transition semiconductors such as ZnO, band gap E_g can be calculated from the following equation [35];

$$(\alpha h\nu)^2 = \beta(h\nu - E_g) \tag{4}$$

where α is optical absorption coefficient, $h\nu$ is photon energy, and β is a constant. The direct band gap is calculated from this equation by extrapolated the straight portion of the $(\alpha h\nu)^2$ plot to the photon energy ($h\nu$) axis. Figure 7 shows the graph of $h\nu$ versus $(\alpha h\nu)^2$ for ZnO thin films with different Ni doping level. The estimated band gap (E_g) are 3.23 eV, 3.11 eV, and 3.15 eV for 0.16 at % Ni ZnO:Ni, 0.20 at.% Ni ZnO:Ni and 0.24 at.% Ni ZnO:Ni, respectively.

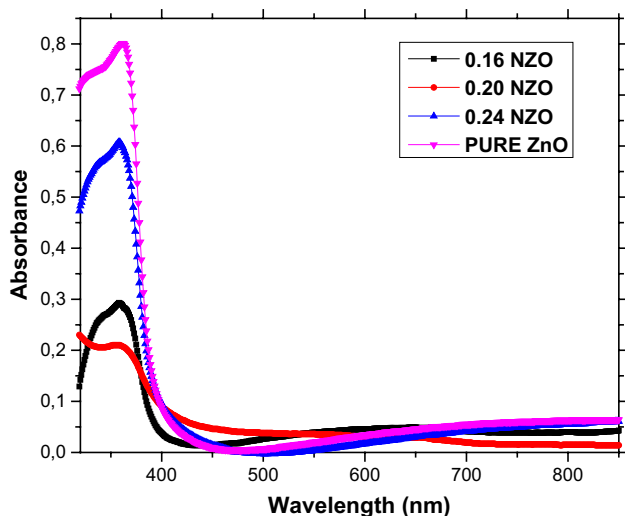


Fig. 5 Absorbance spectra of NZO thin films

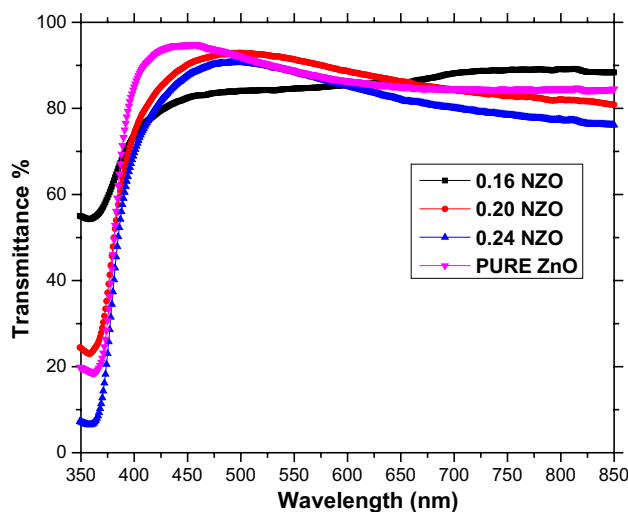


Fig. 6 Transmittance spectra of NZO thin films

The transparent of the films increases relatively with increase of Ni doping level but not this increase is linear. It is thought that the band gap of the thin films increases relatively with increase in Ni content due to Burstein Moss effect [36]. In degenerate semiconductors (ZnO), the optical band gap expands when the carrier concentration increases. It is known as Moss-Burstein effect [37, 38]. In addition, the grain size affects the optical band gap. The effect on grain size and optical band gap is influenced in reverse. In our study, it was found that as the particle size increased, the optical band gap decreased and similarly the optical band gap increased as the particle size decreased. This is in good agreement with the results of our study. It is also believed that the band gap reduction is due to the presence of defects states in the band gap caused by transition dopant ions [39]. Photoluminescence (PL) spectra of the Ni-doped

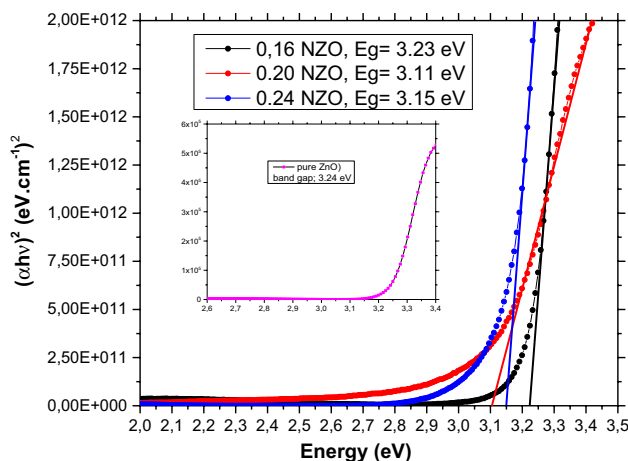


Fig. 7 The plots of $(\alpha h\nu)^2$ versus Energy ($h\nu$) for NZO thin films

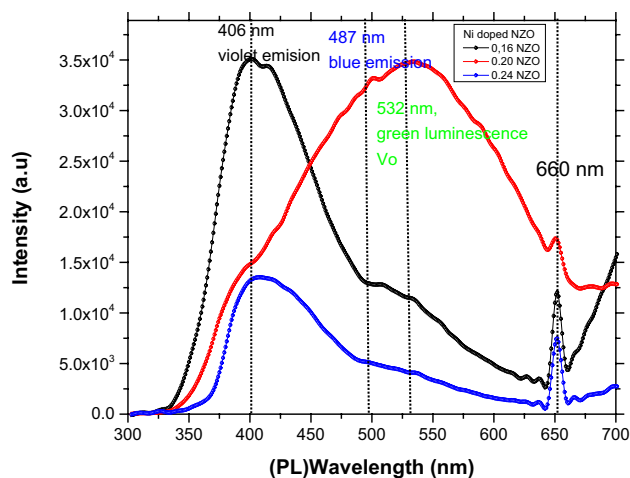


Fig. 8 Photoluminescence spectra of NZO thin films

ZnO films at room temperature is plotted in Fig. 8. The emission band (around 400 nm) for ZnO films with Ni content 0.16 at.% and 0.24 at.% is distinct as compared to other sample. Also, the intensity of this peak for ZnO films with Ni content 0.16 at.% and 0.24 at.% is higher than other sample. The emission of visible light, such as blue and green

luminescence, is attributed to the presence of deep-level emissions (DLE). DLE defects in the ZnO crystal structure are known as oxygen and zinc vacancies (V_O , V_{Zn}), oxygen and zinc interstitials (O_i and Zn_i) and oxygen antisites (O_{Zn}) [40]. It is believed that the emission band centered around at 400 nm could be due to the electron transition from the level of interstitial Zn to the valence band [41, 42]. The decrease in peak intensity might be due to the low number of interstitial atom in the crystal structure [42]. The samples with Ni content 0.16 at.% and 0.24 at.% exhibit a strong blue emission while the other sample exhibits a strong green emission [43]. The another emission band at 660 nm attributed to the presence d-d transition band which is characteristic of Ni (II) with tetrahedral symmetry [44, 45] can be clearly observed in the PL spectrum for all the samples. The UV emission peak in PL spectra shifts to lower energy (red-shift) with increase in Ni content. This red-shift a good accordance with the decrease in band gap (E_g) of the samples with increase of Ni doping level.

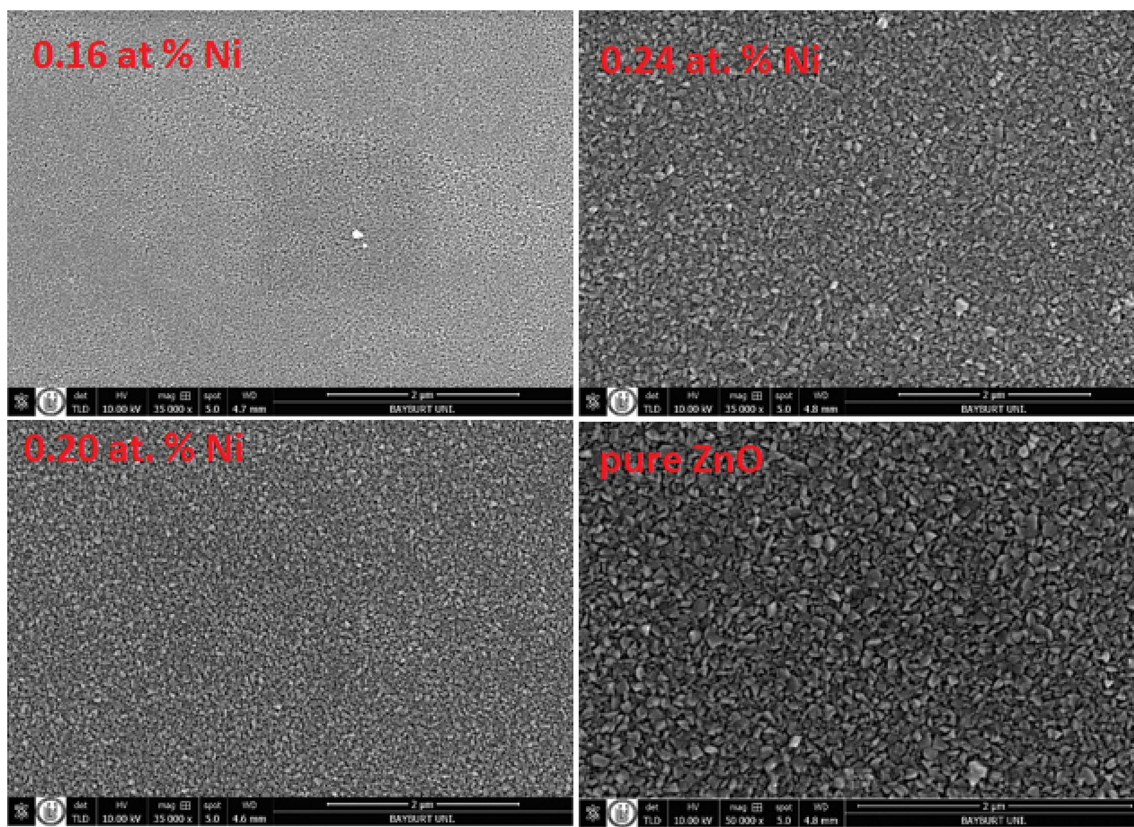


Fig. 9 SEM images of NZO thin films

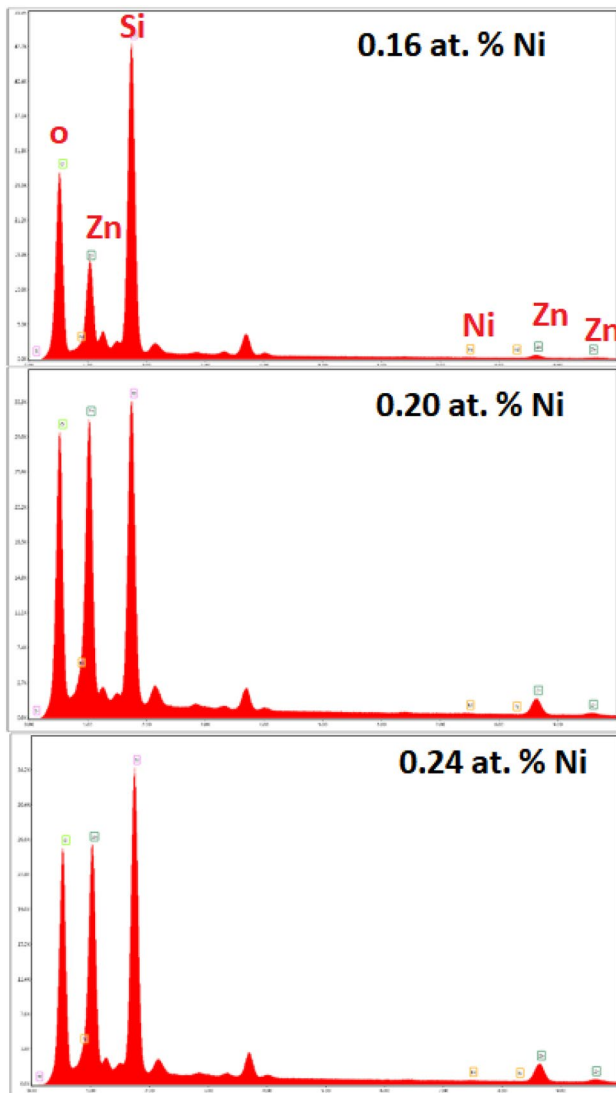


Fig. 10 EDAX images of NZO thin films

3.3 Surface morphology and elemental composition

Morphological and elemental compositions of Ni doped and pure ZnO thin films were investigated using SEM (Fig. 9) and EDX (Fig. 10), respectively. From the SEM images, it can be seen that the surface morphology of all the samples is made up of firmly packed shaped granular grains without any defects (voids, cracks, etc.). More, the granular grains are uniformly distributed with a smooth surface similar to is morphology of the un-doped and Ni or Mn doped ZnO thin films in which was previously reported by Yan et al. [46]. Moreover, the grain size of the samples with Ni content 0.20 at.% and 0.24 at.% is greater than the other sample. In addition, nano-sized plates rather than granular structures were observed due to the increased Ni doping level

[47]. Consequently, the average crystallite size increased linearly with the increase of the Ni doping level, this is confirmed by the XRD results described above. Nickel (Ni), zinc (Zn), oxygen (O), and silicon (Si) in the samples were detected and the Ni content of the ZnO films was estimated by means of EDX spectroscopy (Fig. 10). The Ni content of the samples is 0.16 at.%, 0.20 at.% and 24 at.%, respectively, depending on the increased DC power.

4 Conclusion

NZO and pure ZnO thin films were successfully fabricated by Magnetron sputtering technique. The XRD spectra of thin films reveal that thin films have Wurtzite structure and (002) preferential orientation. The average crystallite size of the thin films was determined as 7.041 nm, 8.463 nm and 9.578 nm with the increased Ni doping rate, respectively, and this value was 26.53 nm for pure ZnO thin film. SEM analyzes showed that the thin films had nano-grain morphology and the average crystallite size was approximately consistent with the XRD results. UV–Vis spectroscopy revealed that the thin films were optically transparent in the visible region and that the optical band gap of the thin films changed significantly with Ni doping. The optical and structural properties of NZO thin films indicate that it can be an alternative material for solar cell applications. In particular, it is thought that it can be used as photoanode materials in dye sensitized solar cell applications due to the fact that it is composed of nanograins having large surface area.

References

1. J. Song et al., Bicolor light-emitting diode based on zinc oxide nanorod arrays and poly (2-methoxy, 5-octoxy)-1, 4-phenylenevinylene. *J. Electron. Mater.* **41**(3), 431–436 (2012)
2. J. Huang, Z. Yin, Q. Zheng, Applications of ZnO in organic and hybrid solar cells. *Energy Environ. Sci.* **4**(10), 3861–3877 (2011)
3. T. Xu et al., The compatibility of ZnO piezoelectric film with micromachining process. *Sens. Actuators A* **104**(1), 61–67 (2003)
4. G. Hirata et al., Synthesis and optoelectronic characterization of gallium doped zinc oxide transparent electrodes. *Thin solid films* **288**(1–2), 29–31 (1996)
5. B. Nasr et al., Electrical resistivity of nanocrystalline Al-doped zinc oxide films as a function of Al content and the degree of its segregation at the grain boundaries. *J. Appl. Phys.* **108**(10), 103721 (2010)
6. Z. Wang et al., Growth of ZnO: Al films by RF sputtering at room temperature for solar cell applications. *Solid-State Electron.* **53**(11), 1149–1153 (2009)
7. W. Beyer, J. Hüpkes, H. Stiebig, Transparent conducting oxide films for thin film silicon photovoltaics. *Thin Solid Films* **516**(2–4), 147–154 (2007)
8. L.E. Greene et al., General route to vertical ZnO nanowire arrays using textured ZnO seeds. *Nano Lett.* **5**(7), 1231–1236 (2005)

9. C. Huang et al., Low content indium-doped zinc oxide films with tunable work function fabricated through magnetron sputtering. *Semicond. Sci. Technol.* **25**(4), 045008 (2010)
10. C. Klingshirn, The luminescence of ZnO under high one- and two-quantum excitation. *Phys. Status Solidi B* **71**(2), 547–556 (1975)
11. L. Peng et al., Growth and characterization of indium doped zinc oxide films sputtered from powder targets. *J. Wuhan Univ. Technol.-Mater. Sci. Ed.* **32**(4), 866–870 (2017)
12. H. Mahdhi et al., Effect of sputtering power on the electrical and optical properties of Ca-doped ZnO thin films sputtered from nanopowders compacted target. *Opt. Mater.* **45**, 97–103 (2015)
13. H. Mahdhi, K. Djessas, Z.B. Ayadi, Synthesis and characteristics of Ca-doped ZnO thin films by rf magnetron sputtering at low temperature. *Mater. Lett.* **214**, 10–14 (2018)
14. N.-E. Sung, K.-S. Lee, I.-J. Lee, Structural characterization of Zr-doped ZnO films deposited on quartz substrates by reactive radio frequency magnetron co-sputtering. *Thin Solid Films* **651**, 42–47 (2018)
15. X. Jiang et al., Aluminum-doped zinc oxide films as transparent conductive electrode for organic light-emitting devices. *Appl. Phys. Lett.* **83**(9), 1875–1877 (2003)
16. I. Volintiru et al., Evolution of the electrical and structural properties during the growth of Al doped ZnO films by remote plasma-enhanced metalorganic chemical vapor deposition. *J. Appl. Phys.* **102**(4), 043709 (2007)
17. Y. Liu, L. Zhao, J. Lian, Al-doped ZnO films by pulsed laser deposition at room temperature. *Vacuum* **81**(1), 18–21 (2006)
18. Y. Caglar et al., Morphological, optical and electrical properties of CdZnO films prepared by sol–gel method. *J. Phys. D* **42**(6), 065421 (2009)
19. B. Singh et al., Highly conducting zinc oxide thin films achieved without postgrowth annealing. *Appl. Phys. Lett.* **97**(24), 241903 (2010)
20. M.Y. Zhang, G.J. Cheng, Highly conductive and transparent alumina-doped ZnO films processed by direct pulsed laser recrystallization at room temperature. *Appl. Phys. Lett.* **99**(5), 051904 (2011)
21. S. Fernandez, F. Naranjo, Optimization of aluminum-doped zinc oxide films deposited at low temperature by radio-frequency sputtering on flexible substrates for solar cell applications. *Sol. Energy Mater. Sol. Cells* **94**(2), 157–163 (2010)
22. K.H. Kim, R.A. Wibowo, B. Munir, Properties of Al-doped ZnO thin film sputtered from powder compacted target. *Mater. Lett.* **60**(15), 1931–1935 (2006)
23. J.-H. Oh, K.-K. Kim, T.-Y. Seong, Effects of deposition temperatures and annealing conditions on the microstructural, electrical and optical properties of polycrystalline Al-doped ZnO thin films. *Appl. Surf. Sci.* **257**(7), 2731–2736 (2011)
24. H. Ahn et al., Substrate effects on the structural properties of Cd_{1-x}Mn_xTe thin films grown via magnetron Co-sputtering. *J. Korean Phys. Soc.* **67**(4), 668–671 (2015)
25. G. Paul et al., Structural, optical and electrical studies on sol–gel deposited Zr doped ZnO films. *Mater. Chem. Phys.* **79**(1), 71–75 (2003)
26. G. Malik et al., Optical and other physical properties of hydrophobic ZnO thin films prepared by dc magnetron sputtering at room temperature. *J. Appl. Phys.* **122**(14), 143105 (2017)
27. R. Gupta et al., Band gap engineering of ZnO thin films by In₂O₃ incorporation. *J. Cryst. Growth* **310**(12), 3019–3023 (2008)
28. R.J. Tilley, *Crystals and Crystal Structures* (Wiley, New York, 2006)
29. G. Singla, K. Singh, O. Pandey, Williamson–Hall study on synthesized nanocrystalline tungsten carbide (WC). *Appl. Phys. A* **113**(1), 237–242 (2013)
30. E. Keskenler, G. Turgut, S. Doğan, Investigation of structural and optical properties of ZnO films co-doped with fluorine and indium. *Superlattices Microstruct.* **52**(1), 107–115 (2012)
31. H. Morkoç, Ü Özgür, *Zinc Oxide: Fundamentals, Materials and Device Technology* (Wiley, New York, 2008)
32. L. Juárez-Amador et al., Electrical, optical and magnetoresistive behavior of nanostructured ZnO: Cu thin films deposited by sputtering. *J. Mater. Sci.* **29**(18), 15339–15343 (2018)
33. D. Chakraborti, J. Narayan, J. Prater, Room temperature ferromagnetism in Zn_{1-x}Cu_xO thin films. *Appl. Phys. Lett.* **90**(6), 062504 (2007)
34. H. Liu et al., Structural and optical properties of Cu–N codoped ZnO thin films deposited by magnetron cosputtering. *J. Mater. Sci.* **29**(12), 9901–9907 (2018)
35. T. Li et al., Characteristics of Ni-doped ZnO: Al films grown on glass by direct current magnetron co-sputtering. *Thin Solid Films* **515**(7–8), 3905–3909 (2007)
36. B. Pandey et al., Synthesis of nanodimensional ZnO and Ni-doped ZnO thin films by atom beam sputtering and study of their physical properties. *Physica E* **41**(7), 1164–1168 (2009)
37. C.E. Kim et al., Effect of carrier concentration on optical bandgap shift in ZnO: Ga thin films. *Thin Solid Films* **518**(22), 6304–6307 (2010)
38. Y. Ammaih et al., Structural, optical and electrical properties of ZnO: Al thin films for optoelectronic applications. *Opt. Quant. Electron.* **46**(1), 229–234 (2014)
39. S. Mondal, P. Mitra, Preparation of Ni doped ZnO thin films by SILAR and their characterization. *Indian J. Phys.* **87**(2), 125–131 (2013)
40. G. Vijayaprasath et al., Optical and magnetic studies on Gd doped ZnO nanoparticles synthesized by co-precipitation method. *J. Lumin.* **178**, 375–383 (2016)
41. V. Khomchenko et al., Fabrication and properties of ZnO: Cu and ZnO: Ag thin films. *Superlattices Microstruct.* **42**(1–6), 94–98 (2007)
42. A. Farag et al., Photoluminescence and optical properties of nanostructure Ni doped ZnO thin films prepared by sol–gel spin coating technique. *J. Alloy. Compd.* **509**(30), 7900–7908 (2011)
43. S. Brahma et al., Self-assembled ZnO nanoparticles on ZnO microsheet: ultrafast synthesis and tunable photoluminescence properties. *J. Phys. D* **48**(22), 225305 (2015)
44. S. Singh, N. Rama, M. Ramachandra Rao, Influence of d–d transition bands on electrical resistivity in Ni doped polycrystalline ZnO. *Appl. Phys. Lett.* **88**(22), 222111 (2006)
45. R. Siddheswaran et al., Reactive magnetron sputtering of Ni doped ZnO thin film: investigation of optical, structural, mechanical and magnetic properties. *J. Alloy. Compd.* **636**, 85–92 (2015)
46. X. Yan et al., Nanostructure and optical properties of M doped ZnO (M = Ni, Mn) thin films prepared by sol–gel process. *Physica B* **406**(20), 3956–3962 (2011)
47. A. Ismail, M. Abdullah, The structural and optical properties of ZnO thin films prepared at different RF sputtering power. *J. King Saud Univ.-Sci.* **25**(3), 209–215 (2013)